Corrosion Science 261 (2026) 113626

Contents lists available at ScienceDirect

Corrosion Science

journal homepage: www.elsevier.com/locate/corsci

A generalized model of corrosion inhibition efficiency for multilayer adsorption

Anton Kokalj

Department of Physical and Organic Chemistry, Jožef Stefan Institute, Jamova 39, SI 1000, Ljubljana, Slovenia

ARTICLE INFO

Keywords:
Multilayer adsorption
Corrosion inhibition
Surface coverage
Adsorption isotherm
Standard adsorption free energy

ABSTRACT

In a recent study (Kokalj, 2026), a model was developed to map multilayer surface coverage to inhibition efficiency (η). In that model, the corrosion protectiveness of adsorbed molecular layers beyond the first was postulated to follow a Langmuir-like dependence on the number of layers. In the present work, this model is generalized by leveraging an experimental observation that the polarization resistance of Langmuir–Blodgett monolayers increases linearly with the number of deposited monolayers beyond the first. It is shown that the previously developed model is a special case of the more general formulation presented here. Both models predict a characteristic hallmark shape in the c/η versus c plot — where c is the inhibitor concentration — featuring a bent, arching profile above the $c/\eta = c$ line at low concentrations, followed by a linear regime at higher concentrations. The generalized model, however, provides further insight, indicating that the extent of this curvature increases when the contribution of the subsequent layers to inhibition efficiency is strong, or when the first adsorbed layer contributes weakly, a behavior that is consistently reproduced when the model is applied to experimental inhibition efficiency data from the literature. Yet under many conditions, the curvature remains too subtle to allow unambiguous identification of multilayer adsorption based on c/η versus c plots alone.

1. Introduction

In corrosion inhibition studies, the standard adsorption Gibbs energy ($\Delta G^{\ominus}_{\mathrm{ads}}$) is routinely estimated from c/η versus c plots, which are widely interpreted as c/θ plots due to the commonly used approximation $\theta \approx \eta$, where θ denotes the fractional surface coverage. However, this approximation breaks down in the case of multilayer adsorption, since inhibition efficiency is, by definition, confined to values below one (or 100%), whereas surface coverage in multilayer adsorption can grow arbitrarily large. To address this, a model mapping multilayer surface coverage to inhibition efficiency was developed in previous work [1]. Here, inhibition efficiency is expressed as a dimensionless fraction between 0 and 1, which facilitates a more compact mathematical formulation, rather than as a percentage (0%–100%), an equivalent convention differing only by a scaling factor of 100.

That model [1] was based on two key assumptions: (i) the formation of adsorbed molecular layers beyond the first does not affect the corrosion protectiveness of the first adsorbed layer, and (ii) the inhibition efficiency increases smoothly with coverage and asymptotically approaches unity as coverage tends to infinity. The latter reflects the physical expectation that a sample completely covered by an infinitely thick inhibitor multilayer is no longer exposed to the corrosive environment and corrosion should cease. In that formulation, the corrosion protectiveness of subsequent adsorbate layers was assumed to follow a Langmuir-like dependence on the number of layers, while the coverage itself was described using Brunauer–Emmett–Teller (BET) adsorption theory [2]. Adopting the Langmuir-like ansatz enabled the inhibition efficiency expression — otherwise given as an infinite sum within the BET framework — to be written in closed form, yielding a significantly simplified analytical formulation.

In the present work, the postulated Langmuir-like dependence is replaced with a model based on the *corrosion resistance* of subsequent layers. Specifically, an experimental study [3] on Langmuir–Blodgett monolayers demonstrates that the polarization resistance increases linearly with the number of deposited monolayers beyond the first. This dependence satisfies the second assumption mentioned above—namely, that the inhibition efficiency asymptotically approaches unity as coverage tends to infinity. Based on this insight, a new multilayer model is

E-mail address: tone.kokalj@ijs.si.
URL: http://www.ijs.si/ijsw/K3-en/Kokalj.

https://doi.org/10.1016/j.corsci.2026.113626
Received 23 September 2025; Received in revised form 18 December 2025; Accepted 10 January 2026
Available online 12 January 2026

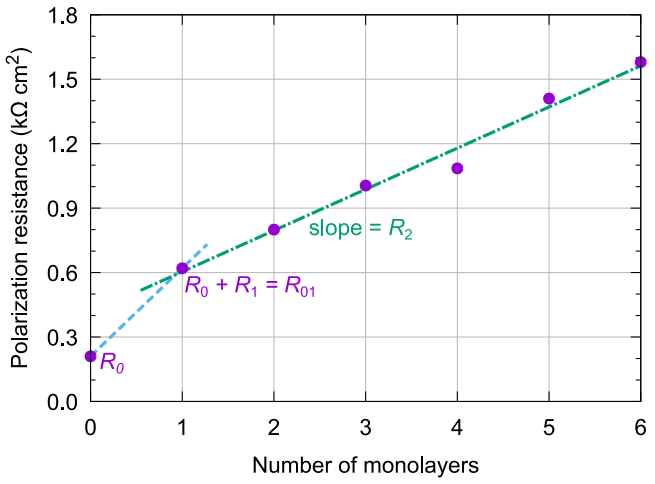

Fig. 1. Polarization resistance measured by Xing et al. [3] (points) as a function of the number of Langmuir–Blodgett monolayers (i) of stearic acid on an Fe electrode in 0.1 M NaCl solution, along with the definitions of R_0, R_1, R_{01}, and R_2 used in the derivation of the corrosion inhibition efficiency multilayer adsorption model. R_2 is determined from the slope of the fitted line for $i > 1$.

derived herein. The previous model [1], which employed the Langmuir-like ansatz, emerges as a special case of the more general model developed in this work.[1] Accordingly, the two are referred to as the special and generalized models, respectively. However, unlike the special model, the general expression for the inhibition efficiency cannot be written in closed form, and the sum must be evaluated explicitly.

2. Theory

In terms of *corrosion resistance*, the inhibition efficiency is defined as:

$$\eta = \frac{R - R_0}{R}, \tag{1}$$

where R is *corrosion resistance* of the inhibited sample and R_0 that of the blank sample. Here, the term *corrosion resistance* is used in a general sense to denote a quantity reciprocal to the corrosion current density, independent of the measurement technique (e.g., LPR, EIS).

Xing et al. [3] demonstrated, using the Langmuir–Blodgett technique to deposit multiple monolayers, that the polarization resistance increases approximately linearly with the number of deposited monolayers (Fig. 1). Hence, the *corrosion resistance* of a sample protected by i monolayers can be expressed as (cf. Fig. 1):

$$R = R_0 + R_1 + (i-1)R_2 = R_{01} + (i-1)R_2 \qquad \text{for } i \geq 1, \tag{2}$$

where R_{01} is a shorthand for the $R_0 + R_1$ sum, R_1 is the *corrosion resistance* of the first (chemisorbed) monolayer, and R_2 is the resistance of a subsequent (physisorbed) monolayer. For i monolayers, there are $i - 1$ such physisorbed monolayers.

Before proceeding with the derivation, a few clarifying remarks are in order. First, the derivation below considers Langmuir–Blodgett monolayers, which simplifies the analysis by allowing the consideration of only complete monolayers. The more general case of non-uniform surface coverage is addressed later in Section 2.2. Furthermore, for practical purposes, the first adsorbed monolayer is referred to as *chemisorbed*, while subsequent layers are referred to as *physisorbed*. This terminology is consistent with the commonly accepted physical picture: many molecules are capable of forming chemisorbed monolayers directly on surfaces, while additional layers are typically stabilized through weaker physisorption interactions. However, it is important to emphasize that the derivation does not depend on this chemisorption/physisorption distinction; the terms are used solely to differentiate the first monolayer from the subsequent ones.

Plugging Eq. (2) into Eq. (1), the inhibition efficiency can be expressed as:

$$\eta = \frac{R_1 + (i-1)R_2}{R_{01} + (i-1)R_2} \qquad \text{for } i \geq 1. \tag{3}$$

This expression can be decomposed into contributions from the first (chemisorbed) monolayer and the subsequent (physisorbed) monolayers:

$$\begin{aligned}\eta &= \frac{R_1}{R_{01} + (i-1)R_2} + \frac{(i-1)R_2}{R_{01} + (i-1)R_2} \qquad \text{for } i \geq 1, \\ &= \eta_1 + \eta_{2\cdots i},\end{aligned} \tag{4}$$

where η_1 is the inhibition efficiency contribution from the first monolayer, and $\eta_{2\cdots i}$ is the contribution from the subsequent monolayers. The latter simplifies to:

$$\eta_{2\cdots i} = \frac{(i-1)R_2}{iR_2 + R_{01} - R_2} = \frac{i-1}{i + R_{01}/R_2 - 1} = \frac{i-1}{i+q} \qquad \text{for } i \geq 1, \tag{5}$$

where:

$$q = \frac{R_{01}}{R_2} - 1. \tag{6}$$

In the previous work [1], a special case with $q = 0$ was considered, yielding $\eta_{2\cdots i} = (i-1)/i$, which corresponds to $R_{01} = R_2$. For efficient corrosion inhibitors, where $R_1 \gg R_0$, this condition implies $R_1 \approx R_2$, meaning that each subsequent monolayer contributes equally to *corrosion resistance* as the first one. In practice, it is reasonable to assume that $R_1 > R_2$, since the first monolayer typically forms stronger, chemisorptive bonds with the surface and directly blocks corrosion reactions, whereas subsequent layers contribute only indirectly by impeding access of corrosive species. This implies that $q > 0$ in most cases.

It can be shown that Eq. (4) is equivalent to the expression used in the previous work [1], where the total inhibition efficiency — denoted here as η_{tot} — was expressed as:

$$\eta_{\text{tot}} = \eta_1^{\max} + (1 - \eta_1^{\max})\eta_{2\cdots i} \qquad \text{for } i \geq 1, \tag{7}$$

where $\eta_1^{\max}$ is the maximum inhibition efficiency of the first layer, corresponding to a complete monolayer. As evident from Eq. (4), the inhibition efficiency of the first monolayer reaches its maximum at $i = 1$. Thus, $\eta_1^{\max}$ is given by:

$$\eta_1^{\max} = \frac{R_1}{R_{01}}. \tag{8}$$

The proof that Eqs. (4) and (7) are equivalent can be shown by direct substitution.

$$\begin{aligned}\eta_{\text{tot}} &= \eta_1^{\max} + (1 - \eta_1^{\max})\eta_{2\cdots i} \\ &= \frac{R_1}{R_{01}} + \left(1 - \frac{R_1}{R_{01}}\right)\frac{(i-1)R_2}{R_{01} + (i-1)R_2} \\ &= \frac{R_1}{R_{01}} + \frac{(i-1)R_2}{R_{01} + (i-1)R_2} - \frac{R_1(i-1)R_2}{R_{01}(R_{01} + (i-1)R_2)} \\ &= \frac{R_1\left(R_{01} + (i-1)R_2\right) + R_{01}(i-1)R_2 - R_1(i-1)R_2}{R_{01}(R_{01} + (i-1)R_2)}\end{aligned}$$

[1] This is not the only instance where a formulation based on *corrosion resistance* yields a Langmuir-like dependence as a special case. Ref. [4] considered the concept of synergism in corrosion inhibition and showed that the synergistic parameter defined with corrosion resistances — the so-called "adjusted 1+1>2" model — is equivalent to that based on the Langmuir model at partial concentrations of inhibitors.

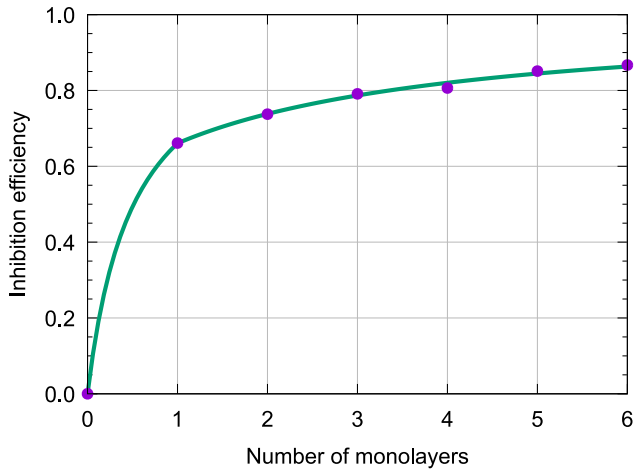

Fig. 2. The experimentally determined corrosion inhibition efficiencies of Xing et al. [3] (points) of Langmuir–Blodgett monolayers of stearic acid on an Fe electrode in 0.1 M NaCl solution. Curve shows the fit using Eq. (10); note that Eq. (7) produces the same result for $i \geq 1$, so the two fitting curves overlap.

$$= \frac{R_1 R_{01} + \cancel{R_1(i-1)R_2} + R_{01}(i-1)R_2 - \cancel{R_1(i-1)R_2}}{R_{01}(R_{01} + (i-1)R_2)}$$
$$= \frac{R_{01}(R_1 + (i-1)R_2)}{R_{01}(R_{01} + (i-1)R_2)} = \frac{R_1 + (i-1)R_2}{R_{01} + (i-1)R_2} = \eta \quad \blacksquare \tag{9}$$

Note that the final equality follows from Eq. (3).

In the previous work [1], the decomposition of the overall inhibition efficiency into contributions from the first and the subsequent layers, as implemented in Eq. (7), was based on the assumption that the adsorbed layers beyond the first do not influence the inhibition efficiency of the first layer. However, the analysis above reveals that it is more precise to state that subsequent layers do not affect the *corrosion resistance* of the first layer. This is because the first term in Eq. (4) depends on the number of layers i, and therefore modifies the inhibition efficiency of the first layer. Nevertheless, the algebraic structure of Eq. (7) remains valid, as demonstrated in Eq. (9).

2.1. Fitting the experimental data

Eq. (3) is formulated for complete monolayers, i.e., for $i \geq 1$. To enable its application to submonolayer coverage ($i < 1$), the expression must be reformulated to explicitly handle this regime. This is achieved by the following modified equation:

$$\eta = \frac{\min(i,1)R_1 + \max(i-1,0)R_2}{R_0 + \min(i,1)R_1 + \max(i-1,0)R_2}. \tag{10}$$

Using this expression, the experimental data of Xing et al. [3] were fitted, with R_0, R_1, and R_2 treated as fitting parameters. In parallel, the same data were also fitted using Eq. (7), with $\eta_1^{\max}$ and q as fitting parameters. The results are shown in Fig. 2, where the curves obtained from the two equations overlap and are therefore visually indistinguishable for $i \geq 1$, since Eq. (7) is defined only for $i \geq 1$; both reproduce the experimental data points nearly perfectly. This confirms the equivalence of Eqs. (4) and (7), as proven in Eq. (9).

It is worth noting that the fit using Eq. (7) yields $\eta_1^{\max} = 0.66$ and $q = 2.38$. This supports the earlier assertion that q is typically greater than zero, as the first (chemisorbed) layer is expected to provide greater *corrosion resistance* than each subsequent physisorbed monolayer.

2.2. From Langmuir–Blodgett monolayers to a general multilayer case

The difference between Langmuir–Blodgett monolayers and a general multilayer case is that in the latter, the surface coverage is allowed to be non-uniform. In the previous work [1], the Brunauer–Emmett–Teller (BET) adsorption isotherm [2] was used to describe multilayer coverage as a function of inhibitor concentration, and the total inhibition efficiency was expressed as the sum of the first-layer contribution (η_1) and that of all subsequent layers ($\eta_{2(+)}$):

$$\eta = \eta_1 + \eta_{2(+)} = \eta_1 + \sum_{i=2}^{\infty} \eta_i, \tag{11}$$

where η_i corresponds to the $\eta_{2(+)}$ component of inhibition efficiency due to the fraction of the surface exclusively covered by i layers. The term η_i was described as [1]:

$$\eta_i = (1 - \eta_1^{\max}) \frac{i-1}{i} \theta_i, \tag{12}$$

and therefore consisted of three components:

- $(1 - \eta_1^{\max}) \equiv$ the maximum value of $\eta_{2(+)}$,
- $\frac{i-1}{i} \equiv$ the protectiveness of the i layers,
- $\theta_i \equiv$ the fraction of the surface exclusively covered by the i layers.

In the previous work [1], the protectiveness component (second item above) was postulated to be $(i-1)/i$ using a Langmuir-like ansatz. This form is algebraically equivalent to the Langmuir isotherm, $\theta = Kc/(1 + Kc)$, with Kc replaced by $i - 1$, and it guarantees that the inhibition efficiency asymptotically approaches unity as the coverage tends to infinity.

The generalized formulation introduced in Eq. (5) reveals that the protectiveness component $(i - 1)/i$ used previously is a special case corresponding to $q = 0$. Hence, the generalized expression for η_i should be used instead:

$$\eta_i = (1 - \eta_1^{\max}) \frac{i-1}{i+q} \theta_i. \tag{13}$$

The $\eta_{2(+)}$ contribution is thus given by:

$$\eta_{2(+)} = \sum_{i=2}^{\infty} (1 - \eta_1^{\max}) \frac{i-1}{i+q} \theta_i. \tag{14}$$

The fraction of the surface θ_i that is exclusively covered by i layers can be described using BET adsorption theory. According to the BET model, the expression for θ_i is:

$$\theta_i = w\theta_0 x^i, \tag{15}$$

where:

$$x = cK_2, \tag{16}$$

$$w = \frac{K_1}{K_2}, \tag{17}$$

$$\theta_0 = \frac{1-x}{1-x+wx} \qquad \text{(valid for } x \leq 1\text{)}. \tag{18}$$

Here, c is the inhibitor concentration in the bulk solution; K_1 is the adsorption equilibrium constant for adsorption on a bare surface (i.e., first-layer adsorption); K_2 is the adsorption equilibrium constant for adsorption onto an adsorbate layer (i.e., subsequent-layer adsorption); and θ_0 is the fraction of the surface not covered by any adsorbate.

Inserting the BET expression for θ_i into Eq. (14), we obtain:

$$\eta_{2(+)} = (1 - \eta_1^{\max}) w\theta_0 \sum_{i=2}^{\infty} \frac{i-1}{i+q} x^i. \tag{19}$$

In the special case of $q = 0$, this sum can be written in closed form and the expression for $\eta_{2(+)}$ becomes [1]:

$$\eta_{2(+)} = (1 - \eta_1^{\max})\, w\, \frac{(1-x)\ln(1-x) + x}{1-x+wx}, \qquad \text{for } x < 1. \tag{20}$$

However, for $q > 0$, the sum in Eq. (19) cannot be expressed analytically. Instead, it must be evaluated explicitly, which effectively leads to the BET-n model [1,5], where n is the maximum number of considered layers. In this case, $\eta_{2(+)}$ becomes:

$$\eta_{2(+)}(n) = (1 - \eta_1^{\max}) w\theta_0(n) \sum_{i=2}^{n} \frac{i-1}{i+q} x^i, \tag{21}$$

where $\theta_0(n)$ is the BET-n fraction of the surface not covered by adsorbates [1]:

$$\theta_0(n) = \frac{1}{1 + w\frac{x(1-x^n)}{1-x}} \tag{22}$$

The final expression for the overall inhibition efficiency is obtained by combining the monolayer model for η_1, developed in Ref. [6], with the above expression for $\eta_{2(+)}$:

$$\eta(n) = \eta_1^{\max}\left(1 - \theta_0(n)^{m/\eta_1^{\max}}\right) + \left(1 - \eta_1^{\max}\right) w\theta_0(n) \sum_{i=2}^{n} \frac{i-1}{i+q} x^i, \tag{23}$$

where m is the number of surface sites protected by a single inhibitor molecule at a very low coverage [6].

Note that due to the finite sum in Eq. (23), the maximum achievable inhibition efficiency is less than one:

$$\eta^{\max}(n) = \lim_{x\to\infty} \eta(n) = \eta_1^{\max} + (1 - \eta_1^{\max})\frac{n-1}{n+q} < 1, \tag{24}$$

which is physically reasonable because $\eta = 1$ requires the coverage to tend to infinity.

2.3. The special case of $q = 0$

In the special case of $q = 0$, the infinite sum in Eq. (19) can be evaluated in closed form, resulting in Eq. (20). However, this expression is valid only for $x < 1$. The reason is that at $x = 1$, the BET coverage becomes infinite, as it is given by [1,2]:

$$\theta = \frac{wx}{(1-x)(1-x+wx)}. \tag{25}$$

Physically, $x = 1$ corresponds to condensation of the adsorbate on the surface, i.e., the onset of unbounded multilayer growth within the BET adsorption model, which occurs at the following concentration (cf. Eq. (16)):

$$c_{\text{cond}} = \frac{1}{K_2}, \tag{26}$$

where the subscript "cond" stands for condensation.[2]

Note also that the logarithmic term $\ln(1-x)$ in Eq. (20) diverges at $x = 1$. To obtain a workable expression at all concentrations, this divergence is avoided by replacing the terms $1 - x$ and $(1-x)\ln(1-x)$ with the functions $t(x)$ and $L(x)$, respectively, defined as [1]:

$$t(x) = \max(1 - x, 0) \tag{27}$$

and

$$L(x) = \begin{cases} (1-x)\ln(1-x) & \text{for } x < 1, \\ 0 & \text{for } x \geq 1, \end{cases} \tag{28}$$

where the latter follows from the fact that $(1-x)\ln(1-x)$ tends to zero as $x \to 1$. Consequently, the expression for θ_0 in Eq. (18) becomes:

$$\theta_0 = \frac{t(x)}{t(x) + wx}, \tag{29}$$

and the expression for $\eta_{2(+)}$ in Eq. (20) is rewritten as:

$$\eta_{2(+)} = \left(1 - \eta_1^{\max}\right) w\frac{L(x) + x}{t(x) + wx}, \tag{30}$$

[2] For surfactant inhibitors, a related surface-aggregation concept is the aggregate transition concentration (ATC) [7], associated with a change in adsorption behavior and often interpreted as a transition from monolayer to multilayer adsorption. The c_{cond} concentration defined here is distinct from ATC, as it marks the divergence of the BET multilayer adsorption model. Both surface condensation and ATC are conceptually different from bulk phenomena such as precipitation upon exceeding solubility or, for surfactants, aggregation above the critical micelle concentration (CMC). Nevertheless, since both phenomena are governed by similar intermolecular interactions, the corresponding characteristic concentrations are often comparable [7].

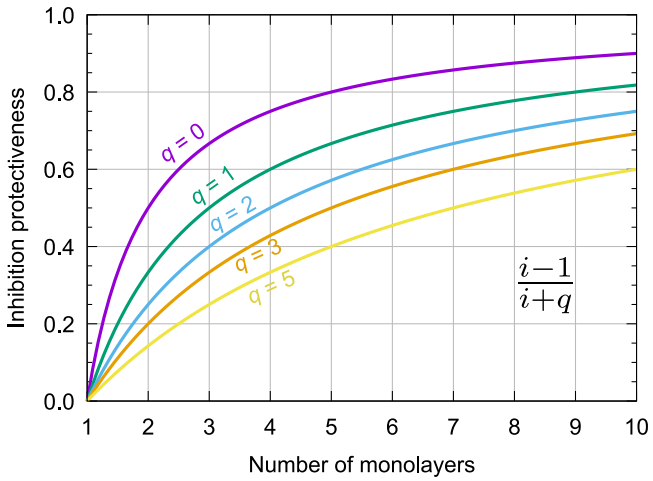

Fig. 3. Dependence of the multilayer corrosion protectiveness, given by $(i-1)/(i+q)$, on the number of monolayers i and the parameter q, for the monolayers physisorbed on top of the chemisorbed monolayer ($i \geq 1$).

which simplifies to:

$$\eta_{2(+)} = 1 - \eta_1^{\max} \qquad \text{for } x \geq 1, \tag{31}$$

whereas for $x < 1$, it behaves as in the original Eq. (20).

Hence, the final BET-based expression for the overall inhibition efficiency in the special case of $q = 0$ is [1]:

$$\eta = \eta_1^{\max}\left(1 - \theta_0^{m/\eta_1^{\max}}\right) + \left(1 - \eta_1^{\max}\right) w\frac{L(x) + x}{t(x) + wx}, \tag{32}$$

where θ_0 is given by Eq. (29).

3. Results and discussion

Before analyzing the generalized model of Eq. (23), let us first examine the protectiveness component of η_i in Eq. (13), specifically how the expression $(i-1)/(i+q)$ depends on the parameter q. This dependence is illustrated in Fig. 3, and the result is quite intuitive: the greater the value of q, the more slowly the protectiveness increases with the number of monolayers i. This behavior can be understood from the definition of q, which is approximately proportional to the ratio R_{01}/R_2 (cf. Eq. (6)). A larger q therefore corresponds to a smaller *corrosion resistance* of the physisorbed monolayer, R_2, relative to the combined resistance R_{01} of the chemisorbed layer and bare surface. Consequently, the smaller the R_2, the more physisorbed monolayers are required to achieve a given level of protection.

Let us now examine the characteristics of the generalized multilayer model of Eq. (23) by analyzing the c/η versus c curve, which is widely interpreted as the c/θ curve due to the common approximation $\theta \approx \eta$. Such plots are routinely used to estimate the standard adsorption Gibbs energy by extrapolating to $c = 0$ and determining the intercept, which is related to the inverse of the adsorption equilibrium constant.

The generalized multilayer model depends on four parameters and two constants: (i) m, the number of surface sites protected by a single inhibitor molecule at very low coverage; (ii) $\eta_1^{\max}$, the maximum achievable inhibition efficiency of the first adsorbed layer; (iii) n, the maximum number of considered layers; (iv) q, a parameter reflecting the relative *corrosion resistance* of physisorbed layers versus combined resistance of the chemisorbed layer and bare surface; (v) K_1, the equilibrium constant for adsorption on the bare surface (i.e., first-layer adsorption); and (vi) K_2, the equilibrium constant for adsorption on an adsorbate layer (i.e., subsequent-layer adsorption).

The adsorption equilibrium constants K_1 and K_2 are calculated from the corresponding standard adsorption Gibbs energies, which are

more intuitive to interpret than the equilibrium constants themselves. As is commonly done, inhibitor adsorption is treated as substitutional adsorption; thus, the relation between the adsorption equilibrium constant and the standard adsorption Gibbs energy ($\Delta G^{\ominus}_{\mathrm{ads}}$) is given by [8]:

$$K_i = \frac{1}{c_{\mathrm{H_2O}}} \exp\left(-\frac{\Delta G^{\ominus}_{i,\mathrm{ads}}}{RT}\right), \qquad \text{for } i = 1, 2, \tag{33}$$

where $c_{\mathrm{H_2O}}$ is the molar concentration of liquid water (55.34 M at 25 °C). In the examples presented below, the values $\Delta G^{\ominus}_{1,\mathrm{ads}} = -30$ kJ/mol and $\Delta G^{\ominus}_{2,\mathrm{ads}} = -20$ kJ/mol are used.

For the analysis of the c/η versus c curves, presented in Fig. 4, the following values of the model parameters are used:

- $m = 1/3$ and 3, to cover two qualitatively different cases: one where an inhibitor molecule only partially protects the site it occupies at low coverage ($m = 1/3$), and another where an inhibitor molecule protects more than one surface site at low coverage ($m = 3$).
- $\eta_1^{\max} = 0.7$ and 0.9, to reflect different relative importance of chemisorbed versus physisorbed layers. A lower value of $\eta_1^{\max}$ corresponds to a lower protectiveness of the chemisorbed layer.
- $n = 10$ and 100, to examine the effect of the maximum number of adsorbed layers. The BET-10 case is included because, in previous work [1], the experimental data [9] were best fitted using the BET-8 based model. The value $n = 100$ is used because it yields results close to the BET model with $n = \infty$ [1].
- $q = 0$, 2, 4, and 6, to span a range from high to progressively lower relative *corrosion resistance* of the physisorbed layer compared to the combined resistance of the chemisorbed layer and bare surface.

In addition to the multilayer model, the single-layer model is also considered in Fig. 4 to highlight the effect of multilayer adsorption on the c/η versus c plot. For the single-layer model, the Langmuir isotherm [10] is used, and the surface coverage is calculated as:

$$\theta_{\mathrm{L}} = \frac{cK_1}{1 + cK_1}, \tag{34}$$

where the subscript L denotes the use of the Langmuir isotherm. The inhibition efficiency is then calculated using the single-layer expression developed in Ref. [6]:

$$\eta_1 = \eta_1^{\max}\left(1 - \theta_{0_{\mathrm{L}}}^{m/\eta_1^{\max}}\right), \qquad \text{where } \theta_{0_{\mathrm{L}}} = 1 - \theta_{\mathrm{L}}. \tag{35}$$

Here, $\theta_{0_{\mathrm{L}}}$ is the fraction of the surface not covered by adsorbates, as given by the Langmuir model.

Fig. 4 reveals that the lower the value of q, the sooner the multilayer model deviates from the monolayer model with increasing concentration. This is easily understood, as a lower q implies higher *corrosion resistance* of a physisorbed layer relative to the chemisorbed one. Hence, multilayer effects become significant at lower inhibitor concentrations. However, near the concentration c_{cond}, corresponding to the onset of unbounded multilayer growth in the BET adsorption model — indicated by the vertical red dashed line — the curves for larger q values exhibit stronger bending, provided that n is large. The reason is that for higher q, the contribution of physisorbed layers to inhibition efficiency is suppressed at low concentrations. But as the concentration approaches c_{cond}, the number of physisorbed layers increases rapidly, and multilayer effects set in abruptly. As a result, the curves for higher q values bend downward sharply near c_{cond}. This pronounced curvature just before c_{cond} is referred to as the *super-coverage* effect.

Despite the super-coverage effect, the overall shape of the c/η versus c curve remains consistent regardless of the value of q. This observation implies that the special case of $q = 0$, developed in the previous publication [1], correctly predicted the characteristic shape: an arching profile above the $c/\eta = c$ line at low concentrations ($c \le c_{\mathrm{cond}}$), followed by a linear regime at higher concentrations.

Note that the effect of multilayer adsorption on the c/η versus c curve diminishes progressively from the top-left plot in Fig. 4 to the bottom-right one. Regarding the curvature of the arching portion of the c/η curve, the figure reveals that this curvature increases when the physisorbed layer contributes more strongly — or, equivalently, when the chemisorbed layer contributes less strongly — to the overall inhibition efficiency. More specifically:

1. The curvature is greater for lower values of $\eta_1^{\max}$. A low $\eta_1^{\max}$ means that the chemisorbed layer alone offers limited inhibition efficiency.
2. The curvature is greater for lower values of m. A small m implies that, at low coverage, each chemisorbed inhibitor molecule weakly protects the surface site to which it is adsorbed.
3. When the number of layers is limited (i.e., for low n), the curvature increases as q decreases. A lower q corresponds to higher *corrosion resistance* of the physisorbed layers relative to the combined resistance of the chemisorbed layer and bare surface, giving rise to more pronounced multilayer effects and stronger curvature.
4. For high values of both $\eta_1^{\max}$ and m — indicating that the chemisorbed layer provides highly efficient protection — the influence of multilayer adsorption becomes insignificant, especially for low n. In this case, the c/η curves appear nearly linear.[3] Only for large q values does a small super-coverage effect become noticeable at high n, as evident in the $n = 100$ case shown in Fig. 4.

Beyond the condensation concentration, the c/η curve follows the $c/\eta = c$ line — marked by the black dashed line in Fig. 4 — if the value of n is large. This occurs because, for large n, the maximum inhibition efficiency approaches unity because the quotient $(n-1)/(n+q)$ tends to one (cf. Eq. (24)). In contrast, for small n, this quotient is significantly less than one, resulting in a maximum inhibition efficiency well below unity. This contrasting behavior is clearly visible in Fig. 4 when comparing the $n = 100$ and $n = 10$ curves.

To supplement the above analysis based on c/η versus c plots, Fig. 5 examines the alternative η versus c representation that can provide complementary insight. In principle, the most direct way to identify multilayer adsorption is to analyze surface coverage as a function of concentration. However, in practical corrosion-inhibition experiments the surface coverage is rarely known explicitly; instead, inhibition efficiency is measured. Because inhibition efficiency is confined to values below one, its bounded nature can considerably mask signatures of multilayer adsorption.

Fig. 5a therefore compares the Langmuir, BET-10, and BET-40 adsorption models on the coverage–concentration plot, where multilayer effects are most clearly revealed. While the Langmuir isotherm saturates at monolayer coverage, the BET-n models, after reaching this point, exhibit a continued increase in coverage with increasing concentration, which is a clear signature of multilayer growth.

Figs. 5b–d show inhibition efficiency as a function of concentration for the BET-40 and BET-10 models. Owing to the bounded nature of inhibition efficiency, the corresponding curves can only partially reflect characteristic multilayer behavior. In particular, for a sufficiently large

[3] Here, the linearity at low concentrations arises from adopting the Langmuir monolayer adsorption model. For a discussion of how the shape and slope of c/θ curves depend on lateral interactions, multi-site adsorption, and surface heterogeneity, see Ref. [8], where it was shown that in many such cases the c/θ curves remain nearly linear. Among these effects, only significant lateral interactions result in pronounced curvature at very low concentrations, in particular attractive interactions, whereas repulsive interactions lead to weaker deviations from linearity.

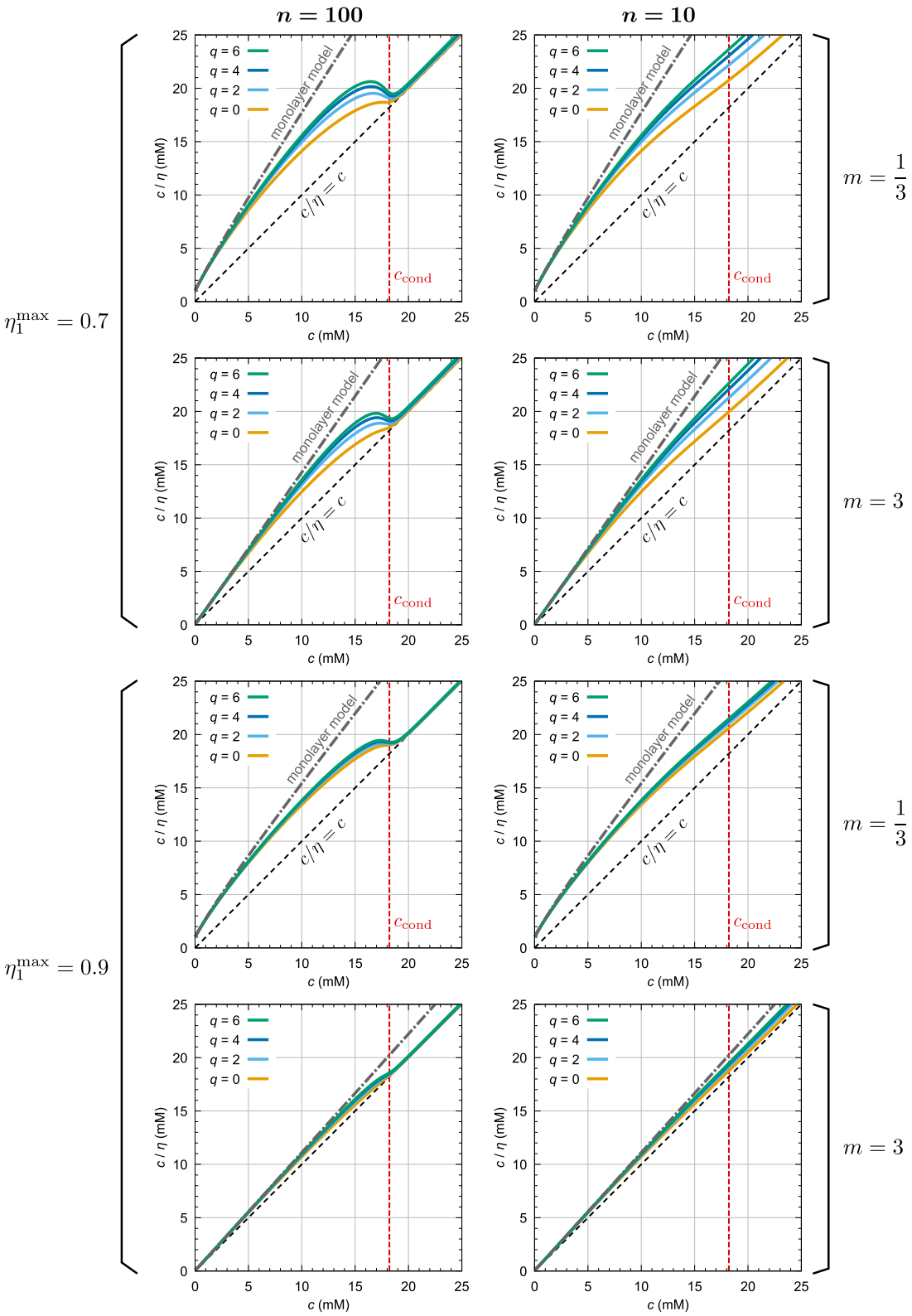

Fig. 4. Dependence of the effect of multilayer adsorption on the c/η versus c plot for the BET-n based models — shown for $n = 100$ (left) and $n = 10$ (right) — with varying q values for $m = 1/3$ and $m = 3$, at $\eta_1^{\max} = 0.7$ (top) and $\eta_1^{\max} = 0.9$ (bottom). The gray dash-dotted line corresponds to the monolayer model. Note that the influence of multilayer adsorption diminishes from the top-left to the bottom-right plot. The vertical red dashed line marks the condensation concentration (c_{cond}) at which the BET theory predicts unbounded multilayer growth. (For interpretation of the references to color in this figure legend, the reader is referred to the web version of this article.)

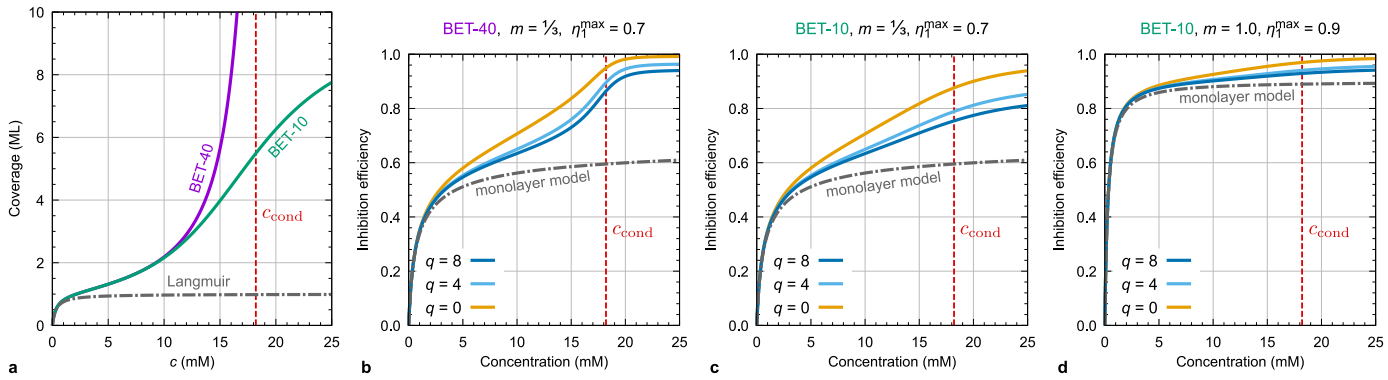

Fig. 5. (a) Surface coverage as a function of inhibitor concentration as predicted by the BET-40, BET-10, and Langmuir adsorption isotherms; (b–d) the corresponding inhibition efficiencies as a function of inhibitor concentration, as predicted by the BET-n-based multilayer models of Eq. (23) and the monolayer model of Eq. (35), for various values of the parameters m, $\eta_1^{\max}$, and q.

number of layers (BET-40) and small values of m and $\eta_1^{\max}$ (Fig. 5b), the η versus c curve exhibits an initial rapid increase followed by a region of reduced slope associated with saturation of the first layer, and a subsequent increase reflecting the formation of additional layers. Such a characteristic shape is a clear sign of multilayer adsorption. However, when the number of layers is small (BET-10), multilayer effects become much less apparent even for small m and $\eta_1^{\max}$ values (Fig. 5c). For larger values of both m and $\eta_1^{\max}$ (Fig. 5d), the multilayer effects are further suppressed, making them almost impossible to identify directly from the η versus c curves alone.

We now evaluate the developed generalized multilayer model using experimental data from the literature for which multilayer adsorption has been inferred. Fig. 6 presents an analysis of inhibition-efficiency data extracted from four independent studies [9,11–13]. The figure is arranged into a matrix of plots with four columns: the top row displays inhibition efficiency as a function of concentration (i.e., η versus c plots), while the second row shows the corresponding c/η versus c plots; the third row provides a zoom to low concentrations for selected cases. The columns, labeled (a)–(d), are ordered from left to right according to decreasing apparent multilayer character.

In Fig. 6a, multilayer effects are most clearly visible. The η versus c curve exhibits a characteristic multilayer shape, while the corresponding c/η versus c plot displays a discernible arching behavior below the condensation concentration c_{cond} (marked by a vertical red dashed line). Although this arching is relatively shallow and therefore not conclusive on its own, the combined evidence from both representations supports multilayer adsorption. In Fig. 6b, the multilayer signature in the η versus c plot is less pronounced but remains suggestive. In this case, however, the arching behavior in the c/η versus c plot is more pronounced than in Fig. 6a, and together the two representations again indicate multilayer adsorption.

In Fig. 6c, the η versus c curve exhibits a monolayer-like behavior, and multilayer adsorption cannot be inferred directly. Nevertheless, the corresponding low-concentration c/η versus c plot shows an arching shape, thereby providing non-conclusive evidence for multilayer adsorption that would be missed if only the η versus c representation was considered. In contrast, Fig. 6d shows neither a characteristic multilayer shape in the η versus c plot nor a clear arching behavior in the (low-concentration) c/η versus c plot. In this case, the data are well described by the monolayer model of Eq. (35), implying that further evidence would be needed to deduce multilayer adsorption.

The model parameters obtained by fitting the experimental data with the generalized multilayer model are also reported in Fig. 6. Inspection of these values shows that $q > 0$ in all cases, consistent with the reasoning in the theory section, while lower $\eta_1^{\max}$ generally makes multilayer effects easier to recognize in the η versus c plots, consistent with the trends discussed for Fig. 5. However, the analysis presented in Figs. 4–6 demonstrates that the characteristic shapes of the curves are more informative than the specific numerical values of the fitted parameters. Furthermore, fitting experimental data with the developed model is not trivial. First, the model depends on four parameters (n, m, $\eta_1^{\max}$, and q) and two constants (K_1 and K_2). Second, the governing equation is not a closed-form expression but involves a finite sum. Although each parameter has a clear physical interpretation, their number complicates the fitting procedure. In practical applications, the parameters must be constrained to physically meaningful ranges (i.e., $m > 0$, $q \geq 0$, $\eta_1^{\max} \in [0, 1]$, $K_1 \geq K_2 > 0$). When such constraints are applied, the model yields excellent agreement with experiments; for all multilayer fits shown in Fig. 6, the coefficients of determination are $R^2 \geq 0.999$.

Due to the multitude of fitting parameters, good fits can be obtained with different combinations of parameter values, corresponding to multiple local minima in parameter space. Importantly, this non-uniqueness does not affect the qualitative behavior of the fitted curves or the inferred adsorption regime. For example, the experimental data shown in Fig. 6c were previously fitted [1] using a specialized model with $q = 0$, yielding an excellent description.[4] However, these data are described even better by the generalized model with $q = 10$, further supporting the relevance and flexibility of the generalized formulation.

The principal utility of the developed multilayer model therefore lies in its ability to provide a qualitative explanation of the signatures of multilayer adsorption in the c/η versus c representation, in particular the arching behavior below c_{cond}. While the shape of the η versus c multilayer curves can be anticipated from the form of multilayer adsorption isotherms and the bounded nature of the inhibition efficiency, this is not the case for the c/η versus c curves. In particular, without an adequate multilayer model, it would be difficult to deduce their arching shape at lower concentrations ($c \lesssim c_{\text{cond}}$).

Finally, we note that experimental data can be fitted either in the η versus c or in the c/η versus c representation, leading to similar but not identical parameter values. In Fig. 6, the fitting was performed using the c/η versus c representation.

4. Conclusions

A generalized model of corrosion inhibition efficiency for multilayer adsorption has been developed, extending the previous work [1], where the corrosion protectiveness of adsorbate layers beyond the first was postulated to follow a Langmuir-like dependence. The generalized

[4] A careful reader may note that the reported R^2 value for the monolayer model in the previous work [1] was 0.959, whereas the corresponding value here is higher (0.9998). This difference arises because the earlier fitting was performed in the η versus c representation, while the present fits were carried out in the c/η versus c representation.

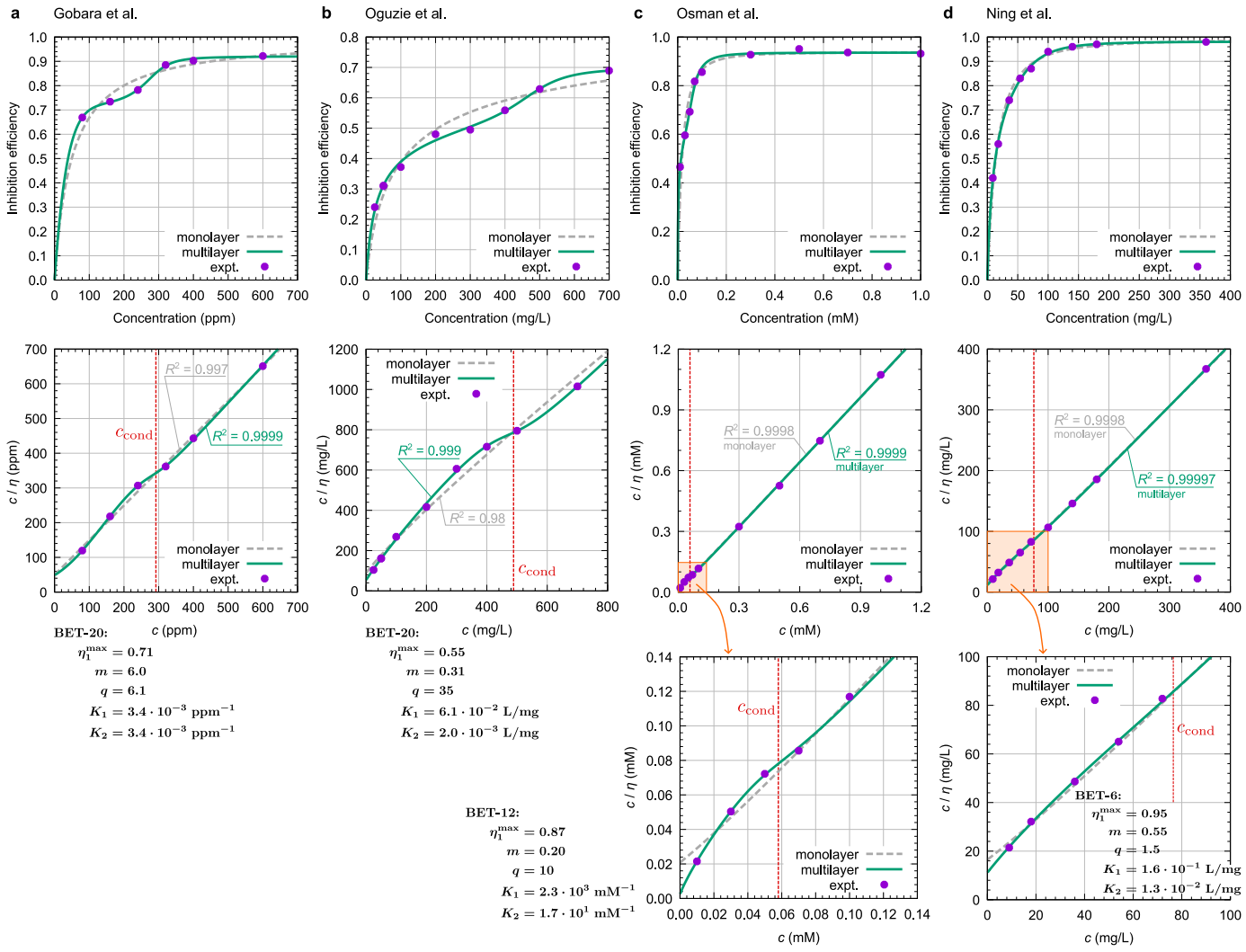

Fig. 6. Validation of the generalized multilayer model using experimental data from (a) Gobara et al. [11], (b) Oguzie et al. [12], (c) Osman et al. [9], and (d) Ning et al. [13]. The top row shows the η versus c plots, while the second row shows the corresponding c/η versus c plots. For panels (b,c), the third row shows a zoom into the low-concentration region to make the arching curvature more apparent. The parameter values obtained from the fits and the corresponding R^2 values are also indicated; all fits were performed in the c/η versus c representation.

model is instead based on a *corrosion resistance* formulation. Both models employ the Brunauer–Emmett–Teller (BET) adsorption theory to describe multilayer coverage; however, the new generalized model more effectively accounts for the relative contribution of physisorbed layers compared to the chemisorbed layer in determining the overall inhibition efficiency. In contrast to the previous model, the generalized model has a clear physical justification and offers a more robust framework for interpreting inhibition efficiency data in the presence of multilayer adsorption. It is shown that the previous model is a special case of the generalized theory, thereby providing a formal justification for the earlier postulate.

Both the special and generalized models predict the characteristic shape of the c/η versus c plot: an arching profile above the $c/\eta = c$ line at low concentrations, transitioning to a linear regime at higher concentrations. The curvature of the arch is governed by the relative importance of physisorbed versus chemisorbed layers, where the chemisorbed layer corresponds to the first adsorbed layer and the physisorbed layers to those beyond it. When the contribution of the physisorbed layers is significant — or conversely, when the chemisorbed layer provides relatively weak protection — the curvature becomes more pronounced. In contrast, as the chemisorbed layer increasingly dominates the inhibition efficiency, multilayer effects progressively diminish and the c/η curves increasingly resemble those of monolayer adsorption, which are often nearly linear.

In contrast to the c/η versus c representation, the qualitative shape of the η versus c multilayer curves can be largely anticipated from the form of multilayer adsorption isotherms combined with the bounded nature of the inhibition efficiency. By comparison, the behavior of the c/η versus c curves is far less intuitive: their curvature and qualitative trends cannot be straightforwardly inferred without recourse to an explicit corrosion inhibition multilayer model. Furthermore, the generalized model reveals that just before the onset of unbound multilayer growth, a sharp downward bending of the curve — termed the *supercoverage* effect — may appear, reflecting a rapid increase in the number of adsorbed layers. However, under many conditions, the curvature remains sufficiently weak to escape detection in experiments — particularly when only a limited number of data points are sampled — thereby contributing to the underappreciation of multilayer adsorption effects in the corrosion inhibition literature.

Finally, the generalized multilayer model was shown to provide a consistently accurate description of experimental inhibition efficiency data reported in the literature, capturing both the overall concentration dependence and the characteristic curvature associated with multilayer adsorption.

AI use statement

The author used ChatGPT (developed by OpenAI) to assist with language editing. All content was created and reviewed by the author, who takes full responsibility for the integrity and accuracy of the manuscript.

Declaration of competing interest

The authors declare that they have no known competing financial interests or personal relationships that could have appeared to influence the work reported in this paper.

Acknowledgments

This work has been financially supported by the Slovenian Research and Innovation Agency (Grant No. P2-0393).

Appendix. Technical details

Graphs were plotted with the Gnuplot software [14] and their post-processing was done in `Inkscape` [15]. Gnuplot was also used for fitting. Derivation of equations was facilitated with WolframAlpha [16].

Data availability

Data will be made available on request.

References

[1] A. Kokalj, Estimating standard adsorption Gibbs energy from corrosion inhibition efficiencies: A case of multilayer adsorption, Corros. Sci. 258 (2026) 113323, http://dx.doi.org/10.1016/j.corsci.2025.113323.
[2] S. Brunauer, P.H. Emmett, E. Teller, Adsorption of gases in multimolecular layers, J. Am. Chem. Soc. 60 (2) (1938) 309–319, http://dx.doi.org/10.1021/ja01269a023.
[3] W. Xing, Y. Shan, D. Guo, T. Lu, S. Xi, Mechanism of iron inhibition by stearic acid Langmuir–Blodgett monolayers, Corrosion 51 (1) (1995) 45–49, http://dx.doi.org/10.5006/1.3293576.
[4] A. Kokalj, Considering the concept of synergism in corrosion inhibition, Corros. Sci. 212 (2023) 110922, http://dx.doi.org/10.1016/j.corsci.2022.110922.
[5] A. Ebadi, J.S. Soltan Mohammadzadeh, A. Khudiev, What is the correct form of BET isotherm for modeling liquid phase adsorption? Adsorption 15 (1) (2009) 65–73, http://dx.doi.org/10.1007/s10450-009-9151-3.
[6] A. Kokalj, On the estimation of standard adsorption free energy from corrosion inhibition efficiencies, Corros. Sci. 217 (2023) 111139, http://dx.doi.org/10.1016/j.corsci.2023.111139.
[7] M.L. Free, A new corrosion inhibition model for surfactants that more closely accounts for actual adsorption than traditional models that assume physical coverage is proportional to inhibition, Corros. Sci. 46 (12) (2004) 3101–3113, http://dx.doi.org/10.1016/j.corsci.2004.03.020.
[8] A. Kokalj, On the use of the Langmuir and other adsorption isotherms in corrosion inhibition, Corros. Sci. 217 (2023) 111112, http://dx.doi.org/10.1016/j.corsci.2023.111112.
[9] M.M. Osman, R.A. El-Ghazawy, A.M. Al-Sabagh, Corrosion inhibitor of some surfactants derived from maleic-oleic acid adduct on mild steel in 1 M H_2SO_4, Mater. Chem. Phys. 80 (1) (2003) 55–62, http://dx.doi.org/10.1016/S0254-0584(01)00588-0.
[10] I. Langmuir, The adsorption of gases on plane surfaces of glass, mica and platinum, J. Am. Chem. Soc. 40 (9) (1918) 1361–1403, http://dx.doi.org/10.1021/ja02242a004.
[11] M. Gobara, B. Zaghloul, A. Baraka, M. Elsayed, M. Zorainy, M.M. Kotb, H. Elnabarawy, Green corrosion inhibition of mild steel to aqueous sulfuric acid by the extract of Corchorus olitorius stems, Mater. Res. Express 4 (4) (2017) 046504, http://dx.doi.org/10.1088/2053-1591/aa664a.
[12] E.E. Oguzie, C.K. Enenebeaku, C.O. Akalezi, S.C. Okoro, A.A. Ayuk, E.N. Ejike, Adsorption and corrosion-inhibiting effect of Dacryodis edulis extract on low-carbon-steel corrosion in acidic media, J. Colloid Interface Sci. 349 (1) (2010) 283–292, http://dx.doi.org/10.1016/j.jcis.2010.05.027.
[13] Z. Ning, Y. Zhu, M.L. Free, Experimental and modeling investigation of pure and mixed surfactant aggregation and associated steel corrosion inhibition in aqueous media, Int. J. Electrochem. Sci. 10 (12) (2015) 10462–10477, http://dx.doi.org/10.1016/S1452-3981(23)11272-7.
[14] T. Williams, C. Kelley, many others, Gnuplot 6.0, 2023, http://www.gnuplot.info/.
[15] Inkscape Project, Inkscape, version 1.4, 2025, https://inkscape.org.
[16] Wolfram Research, Inc., Wolfram| alpha: Computational intelligence, 2025, https://www.wolframalpha.com. Online; (last accessed 31 August 2025).